Incoherent neutrinoproduction of photons and pions in a chiral effective field theory for nuclei

Xilin Zhang and Brian D. Serot

Incoherent Neutrinoproduction of Photons and Pions in a Chiral Effective Field Theory for Nuclei

Xilin Zhang[*] and Brian D. Serot[†]

Department of Physics and Center for Exploration of Energy and Matter

Indiana University, Bloomington, IN 47405

(Dated: August 10, 2012)

Abstract

We study the incoherent neutrinoproduction of photons and pions with neutrino energy $E_\nu \leqslant$ 0.5 GeV. These processes are relevant to the background analysis in neutrino-oscillation experiments, for example MiniBooNE [A. A. Aquilar-Arevalo *et al.* (MiniBooNE Collaboration), Phys. Rev. Lett. **100**, 032301 (2008)]. The calculations are carried out using a Lorentz-covariant effective field theory (EFT) which contains nucleons, pions, the Delta (1232) (Δs), isoscalar scalar (σ) and vector (ω) fields, and isovector vector (ρ) fields, and has $SU(2)_L \otimes SU(2)_R$ chiral symmetry realized nonlinearly. The contributions of one-body currents are studied in the local fermi gas approximation. The current form factors are generated by meson dominance in the EFT Lagrangian. The conservation of the vector current and the partial conservation of the axial current are satisfied automatically, which is crucial for photon production. The Δ dynamics in nuclei, as a key component in the study, are explored. Introduced Δ-meson couplings explain the Δ spin-orbit (S-L) coupling in nuclei, and this leads to interesting constraints on the theory. Meanwhile a phenomenological approach is applied to parametrize the Δ width. To benchmark our approximations, we calculate the differential cross sections for quasi-elastic scattering and incoherent electroproduction of pions without a final state interaction (FSI). The FSI can be ignored for photon production.

PACS numbers: 25.30.Pt; 24.10.Jv; 11.30.Rd; 12.15.Ji

---

[*]Electronic address: `xilzhang@indiana.edu`

[†]Deceased

I. INTRODUCTION

This paper is a continuing work of [1, 2], focusing on neutrinoproduction of photons and pions from nuclei with neutrino energy $E_\nu \leqslant 0.5$ GeV. In Refs. [1, 2], we introduced the Δ resonance as a manifest degrees of freedom to the EFT, known as *quantum hadrodynamics* or QHD [3–10]. (The motivation for this EFT and some calculated results are discussed in Refs. [4, 5, 11–20].) To calibrate the reaction mechanism on the *nucleon* level, we studied the productions from nucleons [2]. The calculations are motivated by the fact that the neutrinoproductions of π^0 and photon from nuclei (and nucleons) are potential backgrounds in neutrino-oscillation experiments, MiniBooNE for example [21–23]. Currently, it is still a question whether the neutral current (NC) photon production might explain the excess events seen at low *reconstructed* neutrino energies, which the MicroBooNE experiment plans to answer [24]. Moreover, Refs. [25–28] point out the possible role of anomalous interaction vertices involving $\omega(\rho)$ Z and γ in NC photon production. So it is necessary to calculate the cross sections for these processes. Here by using the QHD EFT, we study the incoherent productions, in which the nucleus is excited. The other one is the coherent production with the nucleus being intact, which is the topic of future work [1]. We will discuss the power-counting [2] of the calculations through which we will show that the contributions of the anomalous interactions are small in the incoherent NC production of photons (they contribute at next-to-next-to-leading-order). To benchmark the approximation scheme, we study electron scattering in both quasi-elastic and pion production channels.

There have been several experiments measuring the weak response of nuclei across the quasi-elastic region to the Δ excitation peak. In most experiments [30–37], which have ^{12}C and ^{16}O as the primary target nuclei, the mean energy of the beam is around 1 GeV. As emphasized in [2], we expect our theory to work up to 0.5 GeV, so we do not rely on these experiments to constrain the theory at this stage. On the theoretical side, much work has been done, for example in [29, 38–60]. Most of these papers are based on the global or local fermi gas approximation and include contributions from one-body currents, with improved

---

[1] Recently, a unified framework handling the two has been proposed in [29].

[2] In an EFT, there are an infinite number of interaction terms allowed by various constraints. To organize them, we can associate power-counting to each vertex and diagram. The calculation can be done in a perturbative way by summing up diagrams up to some particular power ν. See Refs.[1, 2, 5, 17–20] for detailed discussions about power-counting in QHD EFT.

treatment for FSI and Δ dynamics in the medium. The same approach has also been applied in electron scattering, for example in [61]. In [55–60], scaling approaches are used to address quasi-elastic scattering. Moreover, the contribution from two-body currents was studied nonrelativistically for example in [62]. In the most of these calculations, the Δ dynamics in nuclei is based on the work of [63], in which the Δ self-energy has been studied using a nonrelativistic model. Parallel to the nonrelativistic studies, some work has been initiated in the relativistic framework, QHD EFT, using the local fermi gas (LFG) approximation and including one-body currents [64–68]. The two-body current was investigated relativistically in [69, 70]. These works mainly focus on electron scattering. But the handling of the Δ resonance in these papers is somewhat phenomenological. Moreover in both nonrelativistic and relativistic studies, photon production is rarely investigated.

In this paper, we also apply the LFG approximation [64] to study the one-body current contribution. As shown in [1, 2], we make use of meson dominance to generate form factors for various currents. Because of the built in symmetries in the Lagrangian, the conservation of vector current and the partial conservation of axial current are satisfied. These properties are well preserved in the LFG approximation. Especially for photon production, vector current conservation is crucial. The Δ dynamics, as a key component in this work, is explored to some extent. We introduce interactions between Δ and non-Goldstone meson fields to generate the S-L coupling that has been introduced in phenomenological models [71, 72]. On the other hand, phenomenological knowledge about S-L coupling puts constraints on these couplings. Moreover the Δ decay width increases in the nucleus, because more decay channels are opened up and this effect overcome the reduction of pion decay phase space. Here we follow the phenomenological studies and separate the width to the pion decay width and anything else parameterized by the imaginary part of the Δ spreading potential. As a result of opening new decay channels, the flux having excited a Δ resonance can be transferred to channels that do not involve pion or photon production. Moreover, Pauli blocking can reduce the pion and photon production cross section further, because of the reduction of the final particle's phase space [3]. In this paper, we explore how both Δ and nonresonant contributions are reduced compared to those in free nucleon scattering.

---

[3] The binding effect should be important when the neutrino energy is close to threshold, where the simple approximations used here are not feasible. But this is clearly not important around 0.5 GeV.

However, we do not include FSI effects for pions and knocked out nucleons. The simple treatment can be found in [73, 74], while the complete treatment is implemented in various event generators of experiments, NUANCE for example [75], and GiBUU model [46, 47]. Hence we only compare our predictions with the output of NUANCE *without* FSI [4].

The paper is organized as follows. In Sec. II, we first discuss the LFG approximation and then apply it to electron quasi-elastic scattering, which serves as a benchmark. In Sec. III, the calculation scheme for pion (photon) production is briefly introduced. Then the Δ dynamics is studied with emphasis on the connection between Δ-meson interactions and S-L coupling. The modification of the Δ width is also discussed. After that, electron scattering at the Δ peak is studied, and results are compared with data with explanation of the missing strength. The cross sections of neutrinoproduction of pions are also shown and compared to NUANCE's output. Sec. IV is dedicated to the NC photon production. Finally Sec. V contains a short summary. In the appendices, we show detailed kinematic analyses for both quasi-elastic scattering and pion production.

II.   QUASI-ELASTIC SCATTERING IN LFG APPROXIMATION

This section serves as an illustration of the LFG approximation used for quasi-elastic scattering and for photon and pion production. (See Ref. [2] for discussion on the free nucleon interaction amplitude in all these processes.) Here we make use of the mean-field approximation to calculate the nuclear ground state. The relevant leading order Lagrangian is (the full Lagrangian can be found in [1, 5] for example):

$$\mathcal{L} = \overline{N} \left[i\gamma^\mu \left(\widetilde{\partial}_\mu + ig_\rho \rho_\mu + ig_v V_\mu \right) - M + g_s \phi \right] N \ . \tag{1}$$

The mean-field approximation is presented simply as the follows. Inside the nuclear matter, the vector $\rho^{3\mu}$ and V^μ, and scalar ϕ fields develop nonzero expectation values. In the lab frame of the matter, only two fields (ϕ and V^0) have nonzero values (in the isospin asymmetric case, ρ^0 can also develop a nonzero value). As a result, the nucleon's mass

---

[4] The predictions from NUANCE shown throughout this paper are obtained from the NUANCE v3 event generator [75]. Multiple resonances are considered in NUANCE, but the Δ dominates. The axial mass $M_A^\pi = 1.10 \pm 0.27$ GeV is used which is the same as that used by the MiniBooNE experiment for their *baseline* calculations [76]. However, the actual backgrounds used in their final analyses were scaled to data in a separate exercise.
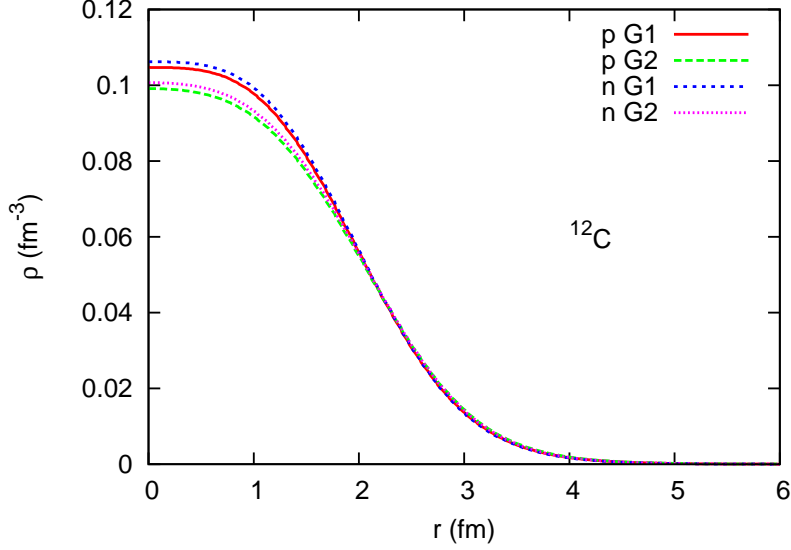
FIG. 1: (color online). Proton and neutron density in ^{12}C with G1 and G2 parameter sets.

is modified: $M^* = M - g_s \langle \phi \rangle$. At the lowest order, the spectrum of nucleons is $E(\vec{p}) = \sqrt{\vec{p}^2 + M^{*2}} + g_v \langle V^0 \rangle$. Inside a finite nucleus, due to different boundary conditions, the mean-field expectation value is space dependent and can be calculated numerically. By using this approximation, we can calculate the bulk properties of the nucleus, the details of which can be found in Ref. [5] for example.

Following [5], we calculate the local density $\rho_{p/n}(\vec{r})$ and field expectation value in ^{12}C (the major nucleus in MiniBooNE's detector). Figs. 1 and 2 show the results based on $G1$ and $G2$ parameter sets in [5]. We will explore the difference due to the two sets in electron's quasi-elastic scattering.

To calculate the electroweak response of nuclei, we use the LFG approximation. This approach has been applied in [64] to study electron quasi-elastic scattering. First, assuming the Impulse Approximation (IA), the interaction happens every time between probe and each individual nucleon This only holds when the transferred momentum is high enough that the interference between different nucleons is reduced due to the big recoil. Second, the response of the nucleus is the incoherent sum of the response of the fermion gas in different regions. This works when the probe's wave length is small enough compared to a characteristic length scale of the nucleus density profile. The discussion can be summarized
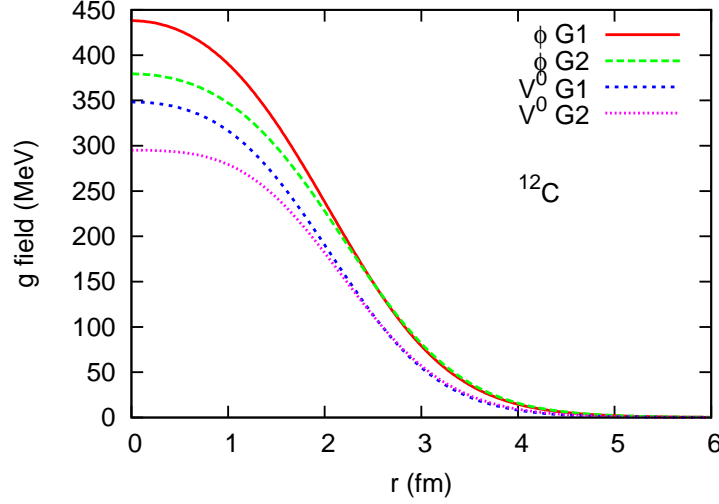
FIG. 2: (color online). $\langle g_s\phi\rangle$ and $\langle g_v V^0\rangle$ in ^{12}C with G1 and G2 parameter sets.
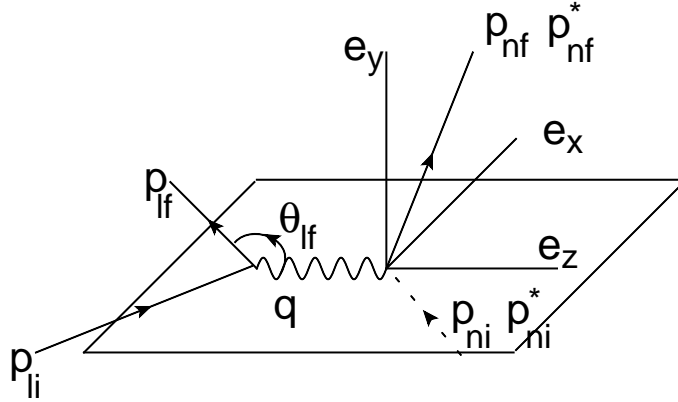

FIG. 3: The kinematics in the lab frame of the nucleus for a lepton interacting with one nucleon inside the nucleus.

in the following equation:

$$\sigma = \int dV \frac{1}{2p_{li}^0} \int \frac{d^3\vec{p}_{nf}^{\,*}}{(2\pi)^3 2p_{nf}^{*0}} \frac{d^3\vec{p}_{lf}}{(2\pi)^3 2p_{lf}^0} \frac{d^3\vec{p}_{ni}^{\,*}}{(2\pi)^3 2p_{ni}^{*0}} (2\pi)^4 \delta^4(q + p_{ni}^* - p_{nf}^*) \sum_{s_f,s_i} |M_{fi}|^2 \ . \quad (2)$$

In this equation, p_{li} and p_{lf} are the incoming and outgoing lepton momentum, $q \equiv p_{li} - p_{lf}$ is the momentum transfer, p_{ni} s_i and p_{nf} s_f are the scattered nucleon's initial and final momentum and spin projection. M_{fi} is the one-body interaction amplitude. The kinematic configuration is shown in Fig. 3. The integration over initial and final nucleon momentum depends on the space dependent Fermi momentum. A detailed discussion about this equation can be found in Appendix A.

The interaction amplitude M_{fi} in Eq. (2) can be expressed in terms of various current

6

matrix elements (V^i_μ A^i_μ and $J_{B\mu}$ are respectively the isovector vector current, isovector axial-vector current and baryon current, $i = \pm 1, 0$ [1, 2]). For electron quasi-elastic scattering (A and B in the state are nucleon isospin),

$$M_{fi} = \frac{e^2}{q^2}\langle J^{(lep)}_{EM\ \mu}\rangle\langle J^{(had)\ \mu}_{EM}\rangle \ ,$$

$$\langle J^{(had)\mu}_{EM}\rangle \equiv \langle N, B|V^{0\mu} + \frac{1}{2}J^\mu_B|N, A\rangle \ ; \tag{3}$$

For charged current (CC) quasi-elastic scattering ($i = \pm 1$, G_F is the Fermi constant and V_{ud} is the u and d quark mixing element in the CKM matrix),

$$M_{fi} = 4\sqrt{2}G_F V_{ud}\langle J^{(lep)}_{Li\mu}\rangle\langle J^{(had)i\mu}_L\rangle \ ,$$

$$\langle J^{(had)i\mu}_L\rangle \equiv \langle N, B|\frac{1}{2}(V^{i\mu} + A^{i\mu})|N, A\rangle \ ; \tag{4}$$

For NC quasi-elastic scattering (θ_w is the weak mixing angle),

$$M_{fi} = 4\sqrt{2}G_F\langle J^{(lep)}_{NC\mu}\rangle\langle J^{(had)\mu}_{NC}\rangle \ ,$$

$$\langle J^{(had)\mu}_{NC}\rangle \equiv \langle N, B|J^{0\mu}_L - \sin^2\theta_w J^\mu_{EM}|N, A\rangle \ . \tag{5}$$

The electroweak currents of leptons are well known, and $\langle N, B|V^i_\mu(J^B_\mu, A^i_\mu)|N, A\rangle$ can be found in [2]. But we need to include the nucleon spectrum modification to the results of [2], which is straightforward complete in the LFG approximation.

A short discussion on FSI is in order here. The picture is the following: the interaction channels are opened in the initial interacting vertex, and then these channels would couple to each other when particles are traveling through the nucleus. The flux among all the initial channels are redistributed due to FSI. This picture is adopted in the GiBUU model calculations for example for CC and NC processes [46] [47]. From conservation of probability, assuming the picture mentioned above is valid, we should expect the sum of these channels in the initial vertex to match the inclusive data. Moreover, Coulomb distortion of the electron is not included in this calculation.

In the upper panels of Figs. 4, 5, and 6, we present differential cross sections $d\sigma/dq^0 d\Omega$ for electron scattering off ^{12}C at given electron energies and scattering angles. In this section we only focus on the so-called quasi-elastic peak at lower energy region, which is believed to be dominated by one nucleon knock out. The higher energy peak will be discussed in Sec. III. In Fig. 4, the electron energy is $E_i = 0.63$ GeV, and the scattering angle is
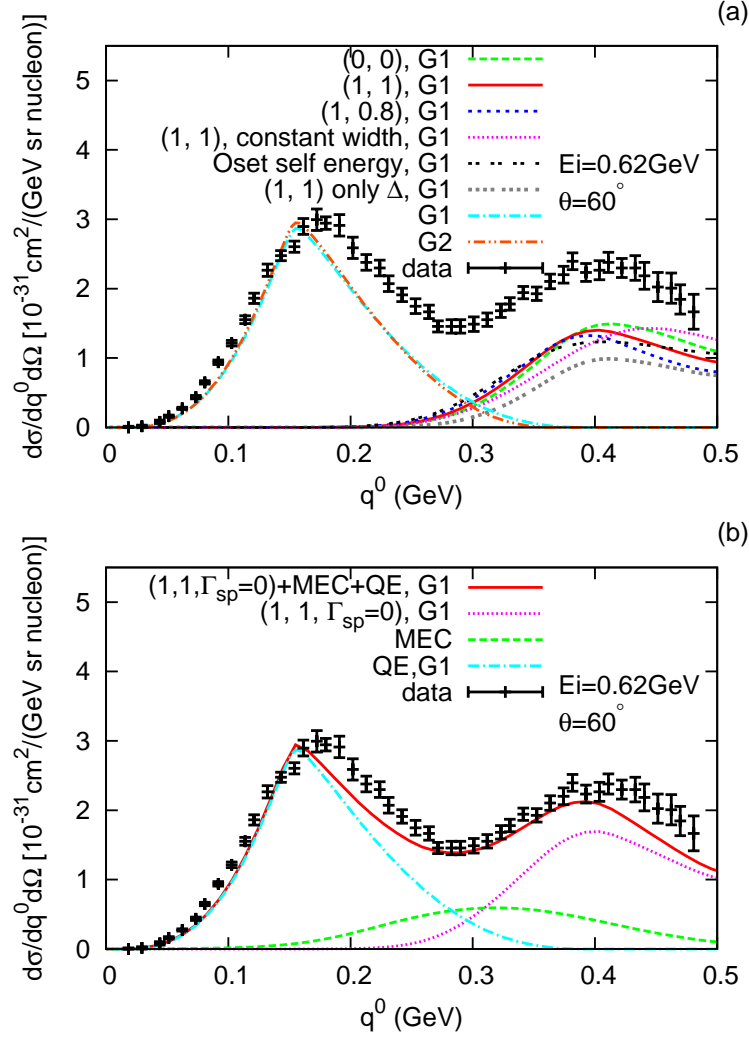
FIG. 4: (color online). Inclusive data for differential cross section of electron scattering off ^{12}C. Incoming electron energy is $E_i = 0.62$ GeV, and scattering angle is $\theta_{lf} = 60°$. The kinematics is measured in the lab frame. Data are from Ref. [77]. Explanations of different plots can be found in the text.

$\theta_{lf} = 60°$. The plots "G1" and "G2" are the calculations done with G1 and G2 parameter sets [5]. The difference between the two is small. The data are from Ref. [77]. The validity of the form factors realized by meson dominance needs to be discussed here. In this figure, $Q^2 \approx 0.3$ GeV^2, $|\vec{q}| \approx 0.55$ GeV at the peak. Below the peak, Q^2 is slightly bigger than 0.3 GeV^2, and above the peak, $Q^2 \leqslant 0.3$ GeV^2. As discussed in [2], meson dominance works when $Q^2 \leqslant 0.3$ GeV^2, and hence can be applied here. This is also true for Figs. 5 and 6. In Fig. 5, the electron energy $E_i = 0.68$ GeV, and the scattering angle $\theta_{lf} = 36°$. In Fig. 6, the electron energy $E_i = 0.73$ GeV, and the scattering angle $\theta_{lf} = 37.1°$. The data are from [77]

FIG. 5: (color online). Inclusive data for differential cross section of electron scattering off ^{12}C. Incoming electron energy is $E_i = 0.68$ GeV, and scattering angle is $\theta_{lf} = 36°$. The kinematics is measured in the lab frame. Data are from [77]. Explanations of different plots can be found in the text.

and [78]. Again, we see only small differences between the "G1" and "G2" parameter sets.
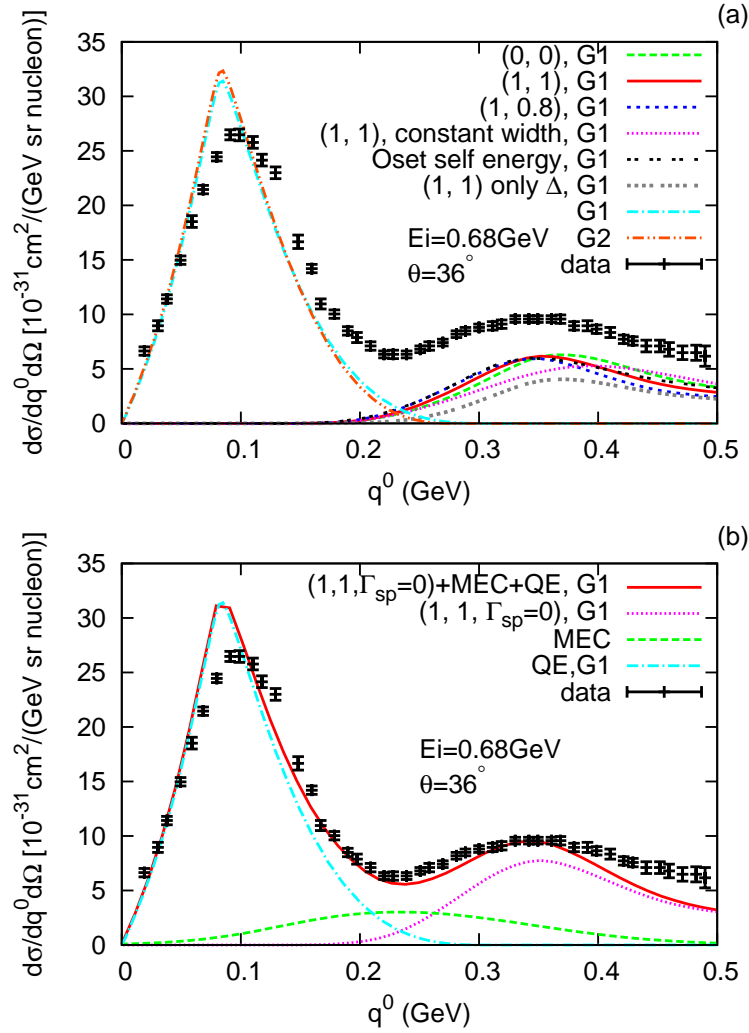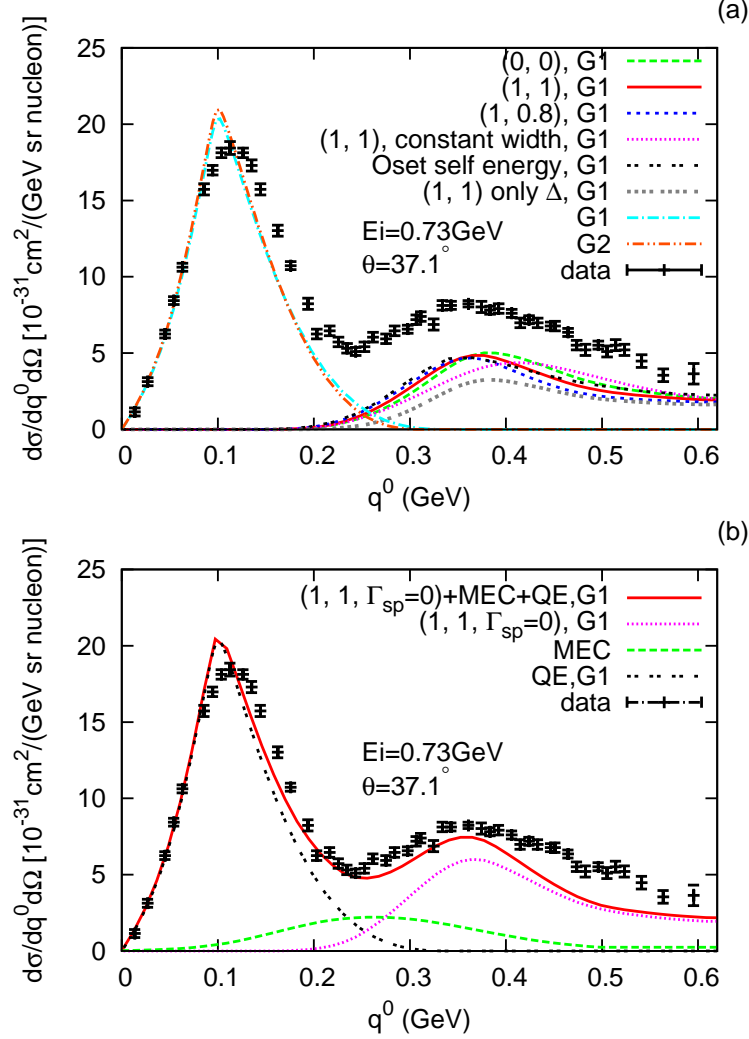
FIG. 6: (color online). Inclusive data for differential cross section of electron scattering off ^{12}C. Incoming electron energy is $E_i = 0.73$ GeV, and scattering angle is $\theta_{lf} = 37.1°$. Data are from [78]. Explanations of different plots can be found in the text.

III. PION PRODUCTION

A. Approximation scheme and Δ dynamics in the nuclear medium

By using the LFG approximation detailed before, the formula for the cross section can be written as

$$\sigma = \int dV \frac{1}{2p_{li}^0} \int \frac{d^3\vec{p}_{nf}^{\,*}}{(2\pi)^3 2p_{nf}^{*0}} \frac{d^3\vec{k}_\pi}{(2\pi)^3 2k_\pi^0} \frac{d^3\vec{p}_{lf}}{(2\pi)^3 2p_{lf}^0} \frac{d^3\vec{p}_{ni}^{\,*}}{(2\pi)^3 2p_{ni}^{*0}}$$

$$\times (2\pi)^4 \delta^4(q + p_{ni}^* - p_{nf}^* - k_\pi) \sum_{s_f, s_i} |M_{fi}|^2 \ . \tag{6}$$
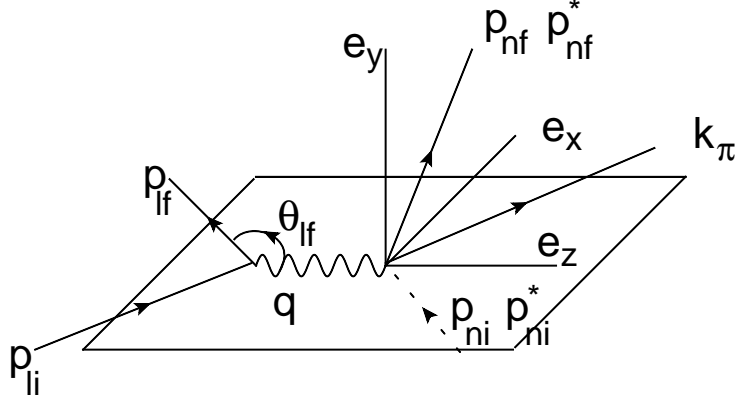
10

FIG. 7: The kinematics in the lab frame of the nucleus for one nucleon inside the nucleus interacting with the lepton and producing a pion.
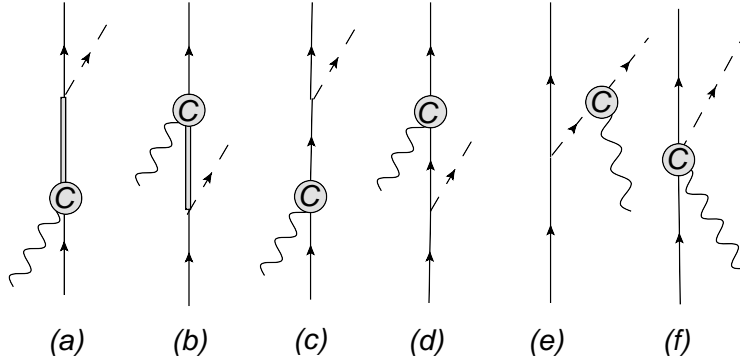

FIG. 8: Feynman diagrams for pion production. Here, **C** stands for various types of currents including vector, axial-vector, and baryon currents. Some diagrams may be zero for some specific type of current. See Ref. [2] for the details.

The details can be found in Appendix B. The notations for various momentum are explained in Fig. 7. All the integrations except the volume integration depend on the space coordinate $\vec{r}$ through the space dependent Fermi momentum. The amplitude M_{fi} in Eq. (6) is similar to those in Eqs. (3), (4), and (5), except that the hadronic currents should be changed to those relevant to pion production:

$$\langle J^{(had)\mu}\rangle \equiv \langle N, \pi | J^{(had)\mu} | N \rangle \ .$$

Several Feynman diagrams contribute here, as shown in Fig. 8, including diagrams with the Δ [(a) and (b)] and all the rest which we define as nonresonant diagrams. See Ref. [2] for details about them. Among the medium-modifications of the matrix elements, the behavior

11

of the Δ needs to be singled out. First, let's focus on the real part of the Δ self-energy. We start from the following Lagrangian (a similar Lagrangian can be found in [68]):

$$\mathcal{L}_{\Delta;\pi,\rho,V,\phi} = \frac{-i}{2}\overline{\Delta}_\mu^a \left\{ \sigma^{\mu\nu} , \left(i\,\widetilde{\partial\!\!\!/} - h_\rho\,\rho\!\!\!/ - h_v\,V\!\!\!/ - m + h_s\phi \right) \right\}_a^b \Delta_{b\nu}$$
$$- \frac{\widetilde{f}_\rho h_\rho}{4m}\overline{\Delta}_\lambda \rho_{\mu\nu}\sigma^{\mu\nu}\Delta^\lambda - \frac{\widetilde{f}_v h_v}{4m}\overline{\Delta}_\lambda V_{\mu\nu}\sigma^{\mu\nu}\Delta^\lambda \; . \tag{7}$$

Here the Δ field is given by the Rarita-Schwinger representation, and $a, b = \pm 3/2, \pm 1/2$ are Δ isospin indices [1]. At the normal nuclear density, the Δ is not stable in nuclear medium. So the expectation values of meson fields are not changed in normal nuclei on mean-field level. Similar to the nucleon case, the Δ spectrum in nuclear matter (without Δ-pion interaction) is given by

$$p_\Delta^0 = h_v\langle V^0\rangle + \sqrt{m^{*2} + \vec{p}_\Delta^2}$$
$$\equiv h_v\langle V^0\rangle + p_\Delta^{*0}$$
$$= h_v\langle V^0\rangle + \sqrt{m^{*2} + \vec{p}_\Delta^{*2}} \; ,$$
$$m^* \equiv m - h_s\langle \phi\rangle \; .$$

The effect of introducing h_s and h_v couplings on the equation of state (EOS) was analyzed in [65, 80, 81]. Some constraints on the couplings, $r_s \equiv h_s/g_s$ and $r_v \equiv h_v/g_v$, were calculated in [65, 81]. Here we resort to the scattering problem to find other constraints. In pion-nucleus scattering studies [71, 72], S-L coupling of the Δ inside the nucleus was introduced by hand, although its origin is not clear in the nonrelativistic model. In this model, a mechanism similar to the generation of the nucleon's S-L coupling is used to generate Δ's. Following discussions in [82] and using the Lagrangian in Eq. (7), we can estimate the S-L coupling of Δ:

$$h_\Delta = \frac{1}{3}\left[\frac{1}{2\overline{m}^2}\frac{d}{r\,dr}\left(h_s\langle\phi\rangle + h_v\langle V^0\rangle\right) - \frac{\widetilde{f}_v}{m\overline{m}}\frac{d}{r\,dr}\left(h_v\langle V^0\rangle\right)\right]\vec{S}\cdot\vec{L}$$
$$\equiv \alpha(r)\vec{S}\cdot\vec{L} \; . \tag{8}$$

Here, $\overline{m} \equiv m - \frac{1}{2}\left(h_s\langle\phi\rangle + h_v\langle V^0\rangle\right)$. In Fig. 9, we compare our estimates of $\alpha(r)$ defined in Eq. (8) with two different phenomenological fits for ^{12}C. We can see our estimates based on three different parameter sets, $r_s = 1$, $r_v = 1$, 0.9, 0.8, and $\widetilde{f}_v = -1.0$, are consistent with
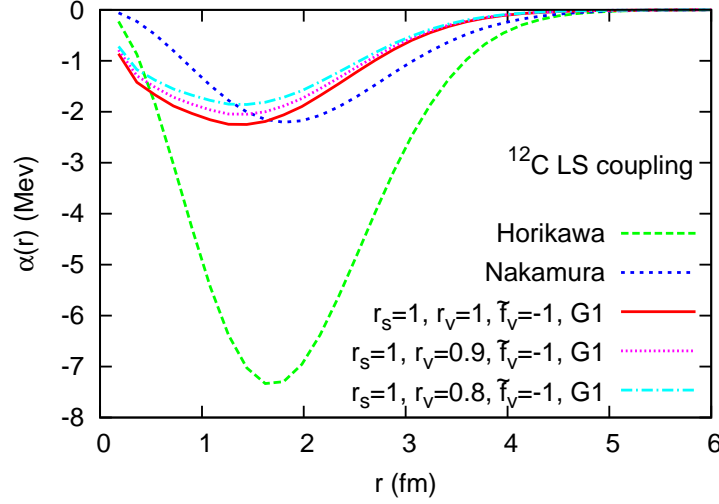
FIG. 9: (color online). The strength of Δ's S-L coupling in ^{12}C. Here we compare two phenomenology results with our three calculations based on different parameter sets. The "Horikawa" is from [72]. The "Nakamura" is from [71]. All these calculations involve setting the G1 parameter to describe the nucleus ground state. We change r_v to 1, 0.9, 0.8 while keeping $r_s = 1$, $\widetilde{f}_v = -1$.

the "Nakamura" result in [71], while the "Horikawa" result in [72] is significantly larger than the "Nakamura" result when $r \geq 1$ fm. Meanwhile, all the couplings are consistent with the "naturalness" assumption, which also motivates our choice of $\widetilde{f}_v = -1$. We do not show the consequence of $r_s = r_v = 0$, since there is no S-L coupling generated in this case.

Secondly, we turn to the imaginary part of the self-energy. It is known that Pauli blocking effects decrease the width due to reduction of the pion-decay phase space, while the collision channels, $\Delta N \leftrightarrow NN$ for example, increase the width. The two competing processes have been investigated in the nonrelativistic models. At normal nuclear density, the net result is to increase the width [63]. In phenomenological fits [79] [72], this increase is taken into account by introducing a density-dependent complex spreading potential for the Δ. Here we follow this approach. Above pion threshold,

$$
\begin{aligned}
\Gamma_\Delta &= \Gamma_\pi + \Gamma_{\rm sp} \, , \\
\Gamma_{\rm sp} &= V_0 \times \frac{\rho(r)}{\rho(0)} \, .
\end{aligned}
\tag{9}
$$

Γ_π is the Δ pion-decay width [63, 66] [5]. $\Gamma_{\rm sp}$ ($V_0 \approx 80$ MeV) is the width in other channels,

---

[5] In the Γ_π calculation, only Pauli-blocking is considered. Modifications of the real part of the nucleon and Δ self-energies are not included.

and has been fitted in [71, 72]. Below pion threshold (useful in photon production),

$$\Gamma_\Delta = \Gamma_{\rm sp} = V_0 \times \frac{\rho(r)}{\rho(0)} . \tag{10}$$

In the cross channel of the Δ diagram, we set the width to zero. Moreover, in the literature [50, 83], the simple increase of the Δ width by $\delta\Gamma \approx 40$ MeV has been used for pion production:

$$\Gamma_\Delta \rightarrow 120 \text{ MeV} + 40 \text{ MeV} . \tag{11}$$

This procedure turns out to work qualitatively as shown later. Furthermore in [61], the Δ self-energy calculated in [63] is used for inclusive electron scattering off nuclei. In Sec. III B, we will compare our results using Eqs. (9) and (10) with those using Eq. (11) and the width in [61, 63].

B. Pion Electroproduction

Here we focus on the region beyond quasi-elastic scattering in the upper panels of Figs. 4, 5, and 6. It is believed that the second peak mainly comes from the Δ excitation inside the nucleus. In the upper panels of these figures, we provide our pion-production results (without FSI) due to six different calculations. We include the full set of Feynman diagrams in the first five calculations, and diagrams with Δ in s and u channels in the sixth. The difference among the first three calculations is the choice of (r_s, r_v) parameter sets: $(r_s = 0, r_v = 0)$, $(r_s = 1, r_v = 1)$, and $(r_s = 1, r_v = 0.8)$. In these three, the Δ width shown in Eqs. (9) and (10) is applied. In the fourth calculation, we set $(r_s = 1, r_v = 1)$ and apply the constant shift of the Δ width as shown in Eq. (11). The fifth calculation is done by using the Δ self-energy as calculated in [63, 84], which is essentially repeating the calculations in [61]. The sixth calculation has $(r_s = 1, r_v = 1)$ and uses the same Δ width as used in first three.

First, let's discuss the location of the Δ-peak along the q^0 axis. The different choice of r_s and r_v indicates different binding potentials for Δ. For $(0, 0)$, the real part of the self-energy is the same as in the vacuum without any binding. For $r_s = 1$, Δ has the same attractive potential as the nucleon. The vector part tuned by r_v provides a repulsive potential. So we can see that $(1, 0.8)$ has a deeper binding potential than $(1, 1)$. Hence, $(0, 0)$ is less bound than $(1, 1)$ and $(1, 1)$ less bound than $(1, 0.8)$. In Figs. 4, 5, and 6, the location of Δ peak in

first three calculations indeed follows this argument. (We can estimate the location of the Δ peak in a global fermi gas model [6].) The fourth calculation with (1, 1) and constant width does not give correct peak position in the three figures: It underestimates (overestimates) Δ's contribution on the left (right) side of the peak, because the constant width assumption overestimates (underestimates) Δ's width on the left (right) side. The fifth calculation by using Δ modification calculated in [63, 84] gives correct location of the peak. Comparing the second with the sixth calculation, we can see the significance of nonresonant contributions (they use same set of parameters and Δ's width).

However, the pion production channel could not explain the full strength of the Δ peak. Meanwhile in the so-called "dip" region between the quasi-elastic scattering and the Δ peak, the calculations also miss strength. This indicates we miss other channels from dip region to the Δ peak. Missing strength at the *peak* position can be qualitatively explained by considering the fourth calculation in the upper panels, whose simple treatment of the Δ width makes analysis transparent. According to Eqs. (9) and (11), we estimate 0.04 GeV $\leqslant$ $\Gamma_{\text{sp}} \leqslant 0.08$ GeV in the sense of averaging over ^{12}C, and hence 0.08 GeV $\leqslant \Gamma_\pi \leqslant 0.12$ GeV. The comparable width of other decay channels shows the importance of them to the inclusive data. Moreover there are contributions from two-body currents without Δ as an intermediate state. In the lower panels of Figs. 4, 5, and 6, we add up three different channels: quasi-elastic, pion production, and two-body current contributions (labeled as meson-exchange-current (MEC) in the plots). The label "(1, 1, $\Gamma_{\text{sp}} = 0$)" for pion production assumes $(r_s = 1, r_v = 1)$ and that no new channel takes away the flux from the Δ pion production. The MEC-contributions are from [70] [85]. Here the total strength matches well with the inclusive data. However a detailed study of different channels in the QHD EFT framework is needed to address this issue conclusively.

The difference should be mentioned here, between our calculations and those in [65] where the QHD model is also applied. Ours are strictly based on the field theory, while in [65] the Δ is introduced by hand (they convolute the cross section based on a "stable" Δ theory

---

[6] Following [64], for ^{12}C, we assume a global Fermi gas, with the nucleon effective mass $M^* = 0.75M$, $g_s \langle \phi \rangle \approx 0.235$ GeV, $g_v \langle V^0 \rangle \approx 0.75 g_s \langle \phi \rangle$ (in lab frame), $m^* = m - r_s g_s \langle \phi \rangle \approx 0.995$ GeV$(r_s = 1)$. Meanwhile in s channel, the Δ momentum $p_\Delta^* = q + p_{ni}^* + (1 - r_v) g_v \langle V^0 \rangle$. It is easy to calculate the q^0-location of the peak by setting $p_\Delta^{*2} = m^{*2}$. For $E_i = 0.62$ GeV, $\theta = 60°$ (see Fig. 4), $q^0 = 0.43$ GeV if $r_v = 1$, and $q^0 = 0.39$ GeV if $r_v = 0.8$.

with a Lorentzian weight function). Moreover, we take into account the contribution from other diagrams, which are not considered in [65]. The two results are different somewhat, but our choice $r_s = 1, r_v = 1$, 0.8 are consistent with the analysis in [65].

Moreover, we can see the difference of cross sections obtained using $r_s = 1, r_v = 1$, 0.8 are not significant, which indicates the total cross sections of neutrinoproduction processes are not sensitive to them either. This will be confirmed by the results in Sec. III C.

C.   CC and NC pion production

Fig. 10 shows the total cross section averaged over proton or neutron number for CC pion production in (anti)neutrino–^{12}C scattering. We also compare our result with NUANCE's output without FSI. In each figure, our calculations including different diagrams and using different r_s and r_v are shown. The "only Δ" calculation only takes into account Δ diagrams. In the others, all the diagrams up to $\nu = 2$ are included. Systematically in all the channels, our "only Δ" calculation is close to the NUANCE output. But other diagrams contained in "$\nu = 2$" calculations are not negligible in all the channels around the resonance region, especially when the s-channel Δ contribution is suppressed by the small Clebsch-Gordan coefficients (for example $\nu_\mu + n \longrightarrow \mu^- + p + \pi^0$). In the very low energy region away from the resonance, the nonresonant diagrams dominate. See [2] for the power counting of diagrams. Moreover, we check that the contributions of higher order ($\nu \geqslant 3$) diagrams are tiny. We also can see that below 0.5 GeV, the ($r_s = 1$, $r_v = 0.8$) results are bigger than the (1, 1) and the (1, 1) are bigger than (0, 0). Following the discussions in Sec. III B about the location of the Δ peak in pion electroproduction, we expect that at a given energy, Δ excitation occupies more phase space in (1, 0.8) than in (1, 1), and more in (1, 1) than in (0, 0). So the pattern among the three different calculations is consistent with the qualitative analysis. Here (0, 0) is presented simply for the purpose of comparison, and its conflict with the Δ S-L coupling is presented in Sec. III A.

One question needs to be raised: do we have Δ-dominance in the *nuclear* scattering around 0.5 GeV ? If we compare the "$\nu = 2$" calculations with "only Δ" calculations in every channel, the answer is no. It turns out the Δ contribution is strongly reduced due to the broadening of its width, compared to its contribution in free nucleon scattering. Meanwhile the nonresonant contributions are reduced due to the Pauli blocking. To see this
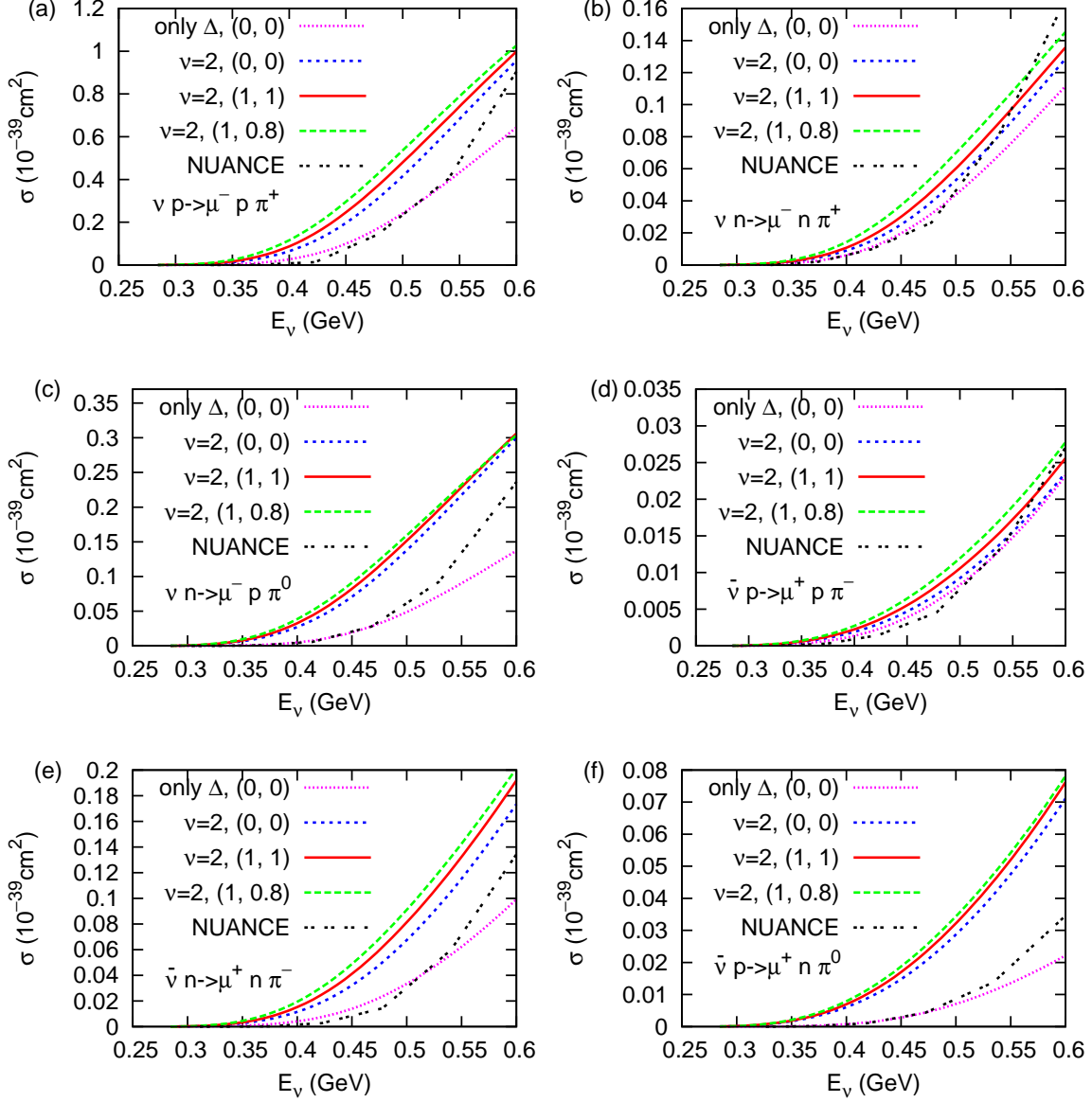
FIG. 10: (color online) Total cross section per proton or neutron for the incoherent CC pion production in neutrino– and antineutrino–^{12}C scattering.

qualitatively, compare our results here with the cross sections shown in [2] for production from free nucleons. In [2], two different calculations can be found, including "only Δ" and "$\nu = 2$". We just show the total cross sections at $E_\nu = 0.5$ GeV in Tab. I for neutrino scattering. For example, "$p, p\pi^+$" indicates the channel $\nu + p \to \mu^- + p + \pi^+$. "(f)" and "(b)" correspond to scattering from free nucleons and from bound nucleons in ^{12}C respectively. In both "only Δ (b)" and "$\nu = 2$ (b)", $r_s = r_v = 1$ (calculations with only Δ and $r_s = r_v = 1$ are not shown in the figures). The "nonres (b)" is the difference between the two, and can

17

$\sigma(10^{-39}cm^2)$	only Δ (f)	$\nu = 2$ (f)	nonres (f)	only Δ (b)	$\nu = 2$ (b)	nonres (b)
$p, p\pi^+$	0.56	0.85	0.29	0.33	0.48	0.15
$n, n\pi^+$	0.088	0.105	0.017	0.056	0.060	0.004
$n, p\pi^0$	0.117	0.258	0.141	0.069	0.153	0.084

TABLE I: Total cross sections averaged over number of proton or nucleon for CC pion production in neutrino–^{12}C scattering at $E_\nu = 0.5$ GeV. See the text for detailed explanations. In the nuclear scattering, $r_s = r_v = 1$.

be viewed qualitatively as the contributions of the nonresonant diagrams [7]. The labeling for free nucleon scattering is the same. We can see that the Δ contribution in nuclear scattering has been reduced systematically by around 50% in all channels, compared to its contribution in nucleon scattering; the nonresonant contributions are also strongly reduced. Clearly, the nonresonant contributions are not negligible in both nucleon and nuclei scattering. The same situation happens in the antineutrino scattering channels and hence are not shown explicitly. This points out the importance of including nonresonant contributions in CC pion production.

In Fig. 11, we show the total cross section for NC pion production from ^{12}C. The categorization of the different calculations are the same as those for CC scattering. Again the NUANCE output is close to our "only Δ" calculation. Among the first three calculations in each channel, at fixed (anti)neutrino energy, (1, 0.8) gives bigger a cross section than (1, 1) and (1, 1) bigger than (0, 0). This is the same as in the CC production, which has been explained in terms of kinematics. Moreover, we can see how Δ-dominance is violated in the NC case, as shown in Tab. II (the labellings are the same as those in Tab. I, and free nucleon scattering results are from [2]). The same is true for antineutrino–nucleus scattering.

IV.   NC PHOTON PRODUCTION

In this section, we study NC photon production from ^{12}C. The calculation is done in the same way as in pion production, except that the hadronic current in Eq. (5) is changed to

---

[7] In principle, there are interferences between contributions from Δ and other diagrams. At $E_\nu = 0.5$ GeV, we can assume in most of phase space, the Δ is "on shell" while contributions from other diagrams are real, and hence the interferences are small.
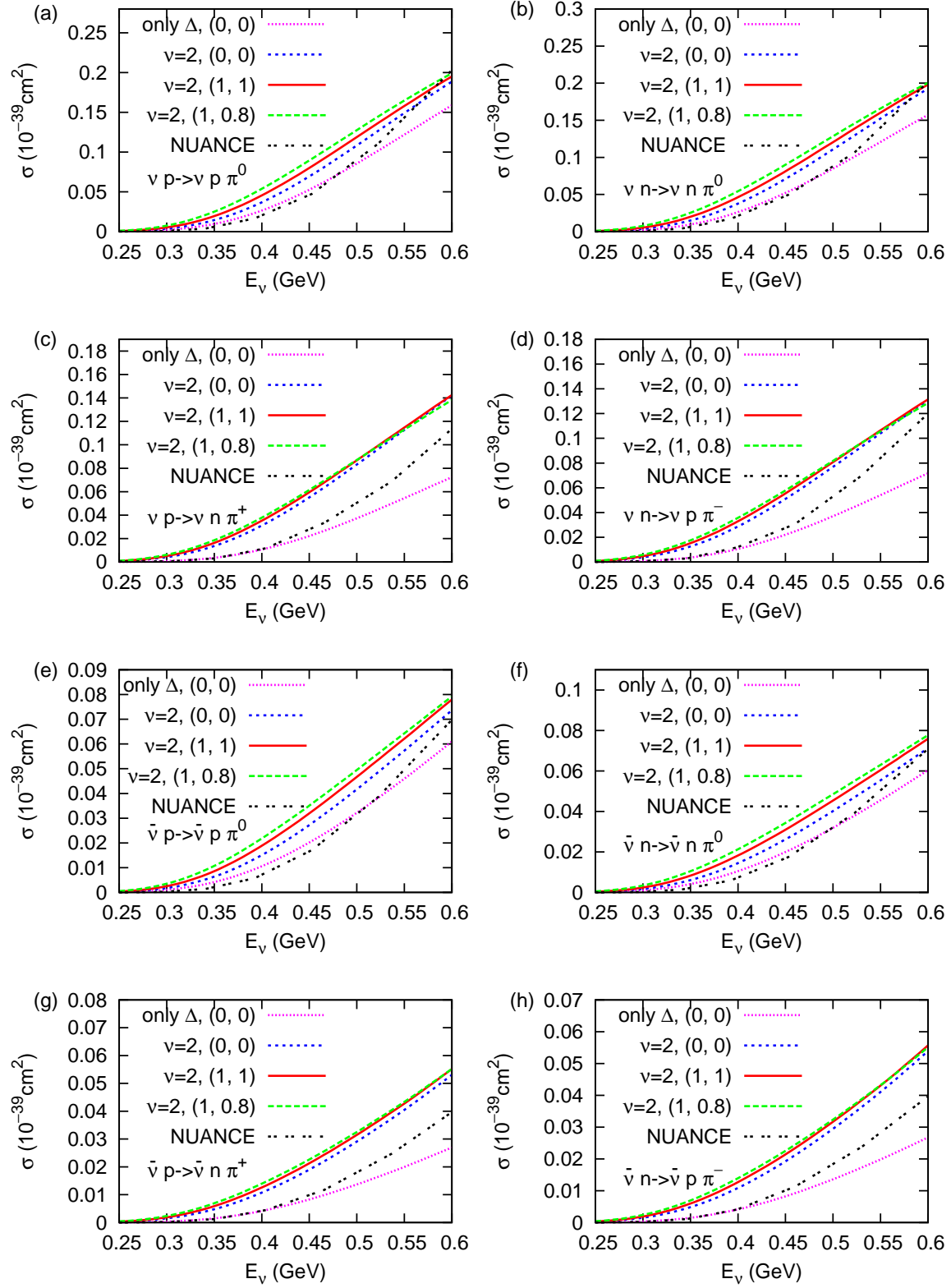
FIG. 11: (color online). Total cross section per proton or neutron for the NC pion production in neutrino– and antineutrino–^{12}C scattering.

$\sigma(10^{-39}cm^2)$	only Δ (f)	$\nu = 2$ (f)	nonres (f)	only Δ (b)	$\nu = 2$ (b)	nonres (b)
$p, p\pi^0$	0.194	0.230	0.036	0.101	0.121	0.020
$n, n\pi^0$	0.194	0.234	0.040	0.101	0.123	0.022
$n, p\pi^-$	0.089	0.149	0.060	0.045	0.082	0.037
$p, n\pi^+$	0.089	0.155	0.066	0.045	0.088	0.043

TABLE II: Total cross sections averaged over number of proton or nucleon for NC pion production in neutrino–^{12}C scattering at $E_\nu = 0.5$ GeV. See the text for detailed explanations. In the nuclear scattering, $r_s = r_v = 1$.

the following:

$$\langle J^{(had)\mu} \rangle \equiv \langle N, \gamma | J^{(had)\mu} | N \rangle \ .$$

The Feynman diagrams are the same as those in Fig. 8 with the final π line substituted by the final γ line. See Ref. [2] for detailed discussion about them. Again we need to implement the change of the baryon spectrum when we apply the formula in [2], as we do in previous calculations. Because of built in symmetries in our model, conservation of the vector current is automatically satisfied, which is important for photon production. The difference in the kinematic analysis, compared to that in pion production, is due to the zero mass of the photon. Moreover, we apply an energy cut on the photon energy in the lab frame, $E_\gamma \geqslant 0.15$ GeV, motivated by the MiniBooNE's detector efficiency. This also eliminates the infrared singularity and simplifies the calculation.

In Fig. 12, the total cross sections averaged over proton or neutron number are shown. Four different calculations are compared. The first "only Δ" is the same as before. "$\nu = 3$" calculations include all the $\nu \leqslant 3$ diagrams. It turns out no $\nu = 2$ contact diagrams contribute, and there are only two $\nu = 3$ contact vertices contributing (See Ref. [2] for details):

$$\frac{c_1}{M^2} \overline{N} \gamma^\mu N \operatorname{Tr}\left(\widetilde{a}^\nu \overline{F}^{(+)}_{\mu\nu}\right) \ , \quad \frac{e_1}{M^2} \overline{N} \gamma^\mu \widetilde{a}^\nu N \overline{f}_{s\mu\nu} \ .$$

As we have checked, the contributions of these two are small compared to those of the Δ and existing nonresonant diagrams, which should be expected according to the power-counting. Here, we have assumed their strength are due to both the ω and ρ meson anomalous interaction vertices ($c_1 = 1.5$ and $e_1 = 0.8$) [2, 27]. Moreover for these calculations, changing
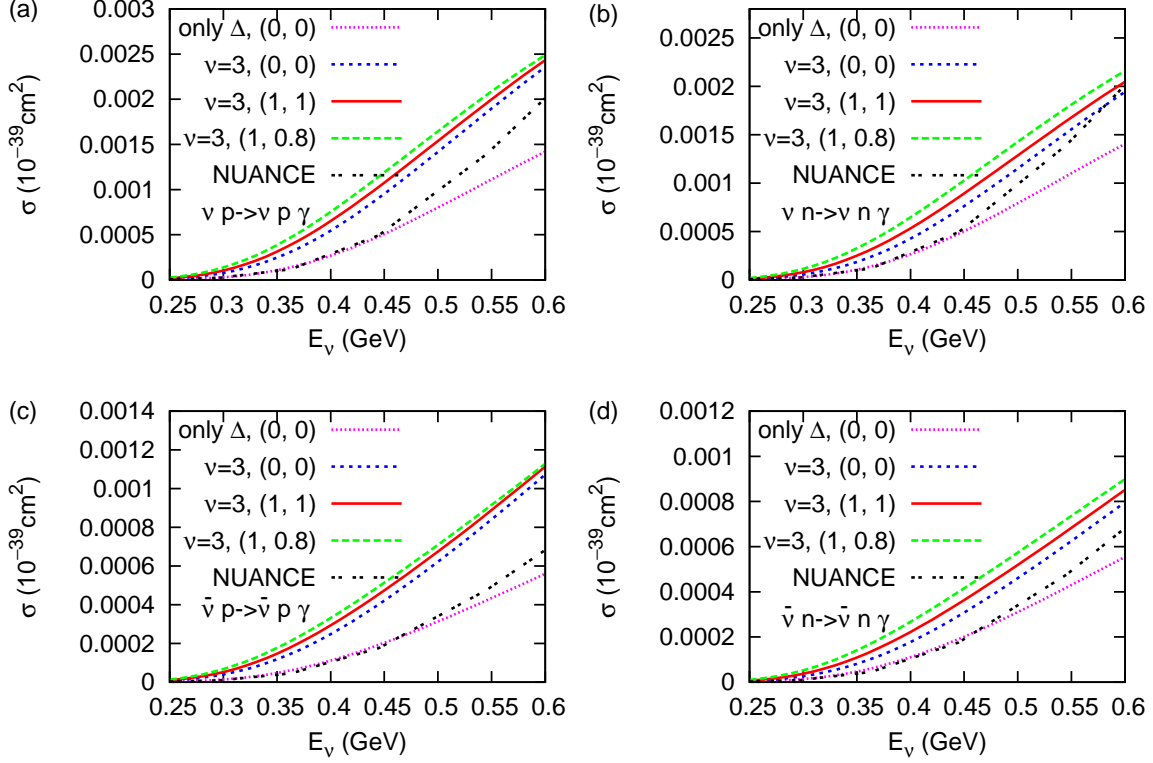
20

FIG. 12: (color online). Total cross section per proton or neutron for the NC photon production in the neutrino– and antineutrino–^{12}C scatterings. Our calculation is done with a photon energy cut $E_\gamma \geqslant 0.15$GeV.

r_s and r_v does not change the total cross section significantly, which is also observed in the differential cross section for pion electroproduction. In the three $\nu = 3$ calculations for different channels, (1, 0.8) gives a bigger cross section than (1, 1) and (1, 1) is bigger than (0, 0). This pattern has been explained in pion production. We also see that the NUANCE output is close to the "only Δ" calculation and smaller than the full calculations, which should be expected from the comparison in pion production.

In addition, in Tab. III we show how the Δ significance changes from neutrino–nucleon scattering to neutrino–nuclus scattering (free nucleon scattering results are from [2] with a change on photon energy cut: $E_\gamma \geqslant 0.15$ GeV): the Δ contribution is strongly reduced, and the nonresonant contribution is reduced less significantly. Since we have put a constraint on the minimum photon energy, the lower energy events are not included in the results and the Pauli blocking effect is not significant. That explains why the nonresonant contribution is not quite suppressed. And the reduction of the Δ contribution is mainly due to the broadening

$\sigma(10^{-42}cm^2)$	only Δ (f)	$\nu = 1$ (f)	nonres (f)	only Δ (b)	$\nu = 1$ (b)	nonres (b)
$p, p\gamma$	1.89	2.49	0.60	0.98	1.50	0.52
$n, n\gamma$	1.89	2.25	0.36	0.97	1.24	0.24

TABLE III: Total cross sections averaged over number of proton or nucleon for NC photon production in neutrino–^{12}C scattering at $E_\nu = 0.5$ GeV. Here $E_\gamma \geqslant 0.15$ GeV for both types of scattering. In the nuclear scattering, $r_s = r_v = 1$.

of its width. We also expect the Pauli blocking effect to be less significant with higher energy neutrinos. Furthermore, the same pattern about the reduction of cross sections happens in antineutrino scattering. Based on Tab. III, we need to include nonresonant contributions in photon production, as emphasized in pion production.

V. SUMMARY

Neutrinoproduction of photons and pions from nuclei provides an important background in neutrino-oscillation experiment and must be understood quantitatively. Especially, we are interested in the possible role of NC photon production in the excess events seen in the MiniBooNE experiment at low *reconstructed* neutrino energy. In Ref. [2], we have calibrated our theory—QHD EFT with Δ introduced—by calculating photon and pion production from free nucleons up to $E_\nu = 0.5$ GeV. In this work, the theory is applied to study the production from nuclei. Here we make use of the LFG approximation and Impulse Approximation, and include only one-body current contributions. In the mean-field approximation of the nuclear ground state, the change of the baryon spectrum is represented by introducing an effective mass for baryons, which leads to the change of one-body currents in this calculation. The calculation for electron quasi-elastic scattering and electroproduction of pion serves as a benchmark for our approximation schemes. We then proceed to calculate the neutrino-production of pion and photon from ^{12}C, and show the plots for total cross section in every channel. First, we present calculations for pion production up to next-to-leading-order with different r_s and r_v parameters as constrained by the phenomenological study. It turns out that total cross sections are not very sensitive to changes of these parameters. Then in NC production of photon, although we show the result up to $\nu = 3$ order, there are no $\nu = 2$ contributions from contact terms, and as we have checked already the $\nu = 3$ contributions

due to c_1 and e_1, related to the so-called anomalous interactions, are tiny (the same has been shown for nucleon scattering in [2]). Again, the total cross section of photon production is not sensitive to choice of different r_s and r_v. In all the plots, the Δ contributions are singled out and compared with the full calculations. Moreover, we also compare our results with the output from NUANCE, and find that the NUANCE output is close to our "only Δ" calculation with ($r_s = 0$, $r_v = 0$) for both pion and photon production, which should be expected since the Δ dominates in NUANCE.

In the calculation, the Δ dynamics in nuclei is a key component. The dynamics has been investigated in a nonrelativistic framework and also initiated in the QHD model. Parallel to the modification of nucleon's spectrum, the Δ-meson couplings (related with r_s and r_v) introduced in our theory dictates the real part of the Δ self-energy. The couplings are used to explain the S-L coupling of Δ. Meanwhile the phenomenological result about S-L coupling based on nonrelativsic isobar-hole models puts an interesting constraint on the Δ-meson coupling strengths, which is complementary to the constraints based on EOS consideration. The Δ width is treated in a simplified way, as we take the advantage of the existing result that shows an increase of the width due to the opening of other decay channels. In pion electroproduction, the pion-production (without FSI) result gives a correct prediction for the location of the Δ-peak. We argue that this deficit is due to the missing of other channels. By adding contributions from two-body currents (from other relativistic study) to our quasi-elastic and pion production (turning off Δ broadening), we can explain the inclusive electron scattering strength. The investigation on Δ dynamics and two-body currents certainly needs to be pursued further in QHD EFT, which plays an important role in nuclear response and other problems.

Moreover, because of the broadening of the Δ width, we expect that in both pion and photon productions, the Δ contribution is much less in nuclear scattering than in nucleon scattering. But the reduction of nonresonant contributions would be less at higher energies (beyond 0.5 GeV), because the Pauli blocking effect should be less important. In Tabs. I, II, and III, we have shown explicitly the cross sections at $E_\nu = 0.5$ GeV due to Δ and nonresonant contributions in both neutrino–nucleon and neutrino–nucleus scattering. Although we see the reduction of nonresonant contributions for pion production in Tabs. I and II, we see a smaller reduction for photon production in Tab. III. This is consistent with the picture that the nonresonant contribution is reduced because of Pauli blocking. The same situation

happens in antineutrino scattering. This conclusion is important for future investigations of higher energy neutrino scattering, which may be relevant to MiniBooNE's excess event problem.

Since our calculation is based on a QHD EFT Lagrangian with all the relevant symmetries built in, the conservation of vector current is manifest. This is crucial for photon production. Also partial conservation of the axial current is a necessary constraint in the problem. By using the mean-field approximation and the LFG model, these constraints are satisfied in a transparent way.

We are currently working on coherent pion and photon production from nuclei by applying this QHD EFT, which may also be relevant to the MiniBooNE low energy excess event problem.

Appendix A: kinematics for quasi-elastic scattering

The analysis of the kinematics is for scattering from nuclear matter, and can be easily generalized in the LFG model. The kinematic variables are shown in Fig. 3, and discussed following Eq. (2). From the mean-field theory in QHD EFT, we know that the leading order Hamiltonian gives rise to the nucleon spectrum in nuclear matter as $p_n^0 = g_v \langle V^0 \rangle + \sqrt{M^{*2} + \vec{p}_n^2}$, $M^* \equiv M - g_s \langle \phi \rangle$. Then we can define $p_n^{*0} \equiv p_n^0 - g_v \langle V^0 \rangle = \sqrt{M^{*2} + \vec{p}_n^2} = \sqrt{M^{*2} + (\vec{p}_n^{\,*})^2}$. This can be generalized from the lab frame to an arbitrary frame. In the LFG model, we consider each neighborhood inside the nucleus as a homogeneous system; the field expectations, $\langle \phi(x) \rangle$ and $\langle V^\mu(x) \rangle$, are space-time dependent (in the lab frame, they only depend on the space coordinate). In the following, we always work in the nuclear lab frame. The covariance of our calculation is more transparent with the $p_n^{*\mu}$ variables than

with p_n^μ. For example energy momentum conservation is $q + p_{ni}^* = p_{nf}^*$.

Next we derive the formula for the total cross section. Suppose M_{fi} is the covariant interaction amplitude between the probe and each individual nucleon with specific initial and final states. We have

$$\sigma = \int dV \frac{1}{2p_{li}^0} \int \frac{d^3\vec{p}_{nf}^*}{(2\pi)^3 2p_{nf}^{*0}} \frac{d^3\vec{p}_{lf}}{(2\pi)^3 2p_{lf}^0} \frac{d^3\vec{p}_{ni}^*}{(2\pi)^3 2p_{ni}^{*0}} (2\pi)^4 \delta^4(q + p_{ni}^* - p_{nf}^*) \sum_{s_f, s_i} |M_{fi}|^2 \ . \ \text{(A1)}$$

Pauli blocking leads to constraints on the integration of p_{ni}^* and p_{nf}^*, i.e. $|\vec{p}_{ni}^*| \leqslant p_F$ and $|\vec{p}_{nf}^*| \geqslant p_F$. Here p_F is the Fermi momentum related with the local density. The two constraints can be expressed by using factors $\theta(p_F^2 + p_{ni}^{*\,2} - (p_{ni}^* \cdot V)^2/V^2)$ and $\theta(-p_F^2 - p_{nf}^{*\,2} + (p_{nf}^* \cdot V)^2/V^2)$. In the following, we will not include them explicitly. We know that

$$\int \frac{d^3\vec{p}_{ni}^*}{2p_{ni}^{*0}} \frac{d^3\vec{p}_{nf}^*}{2p_{nf}^{*0}} \delta^4(q + p_{ni}^* - p_{nf}^*) = \int d\phi_{\vec{p}_{ni}^*} dp_{ni}^{*0} \frac{1}{4|\vec{q}|} \ \Big|_{\cos(\measuredangle \hat{q}\hat{p}_{ni}^*) = (2q^0 p_{ni}^{*0} + q^2)/(2|\vec{q}||\vec{p}_{ni}^*|)} \ .$$

By using this, we have the total cross section as

$$\sigma = \int dV \frac{1}{2p_{li}^0} \int \frac{d^3\vec{p}_{lf}}{(2\pi)^3 2p_{lf}^0} \frac{dp_{ni}^{*0}}{|\vec{q}|} \frac{d\phi_{\vec{p}_{ni}^*}}{16\pi^2} \sum_{s_f, s_i} |M_{fi}|^2 \ . \tag{A2}$$

Meanwhile to make our phase space analysis simple, we can integrate over $d|\vec{q}|$ and dq^0:

$$\sigma = \int \frac{dV}{(2\pi)^4} d\phi_{\vec{p}_{ni}^*} dp_{ni}^{*0} dq^0 d|\vec{q}| \frac{1}{16 p_{li}^0 |\vec{p}_{li}|} \sum_{s_f, s_i} |M_{fi}|^2 \ . \tag{A3}$$

Now, we need to calculate the boundary of the phase space in Eq. (A3). From the lepton kinematics, we can determine the boundary of $|\vec{q}|$ ($p_{li}^0 \equiv E_{li}$):

$$|\vec{q}|_{max} = |\vec{p}_{li}| + \sqrt{E_{li}^2 - M_{lf}^2} \ , \tag{A4}$$

$$|\vec{q}|_{min} = |\vec{p}_{li}| - \sqrt{E_{li}^2 - M_{lf}^2} \ . \tag{A5}$$

For a given $|\vec{q}|$, we have the following constraints based on the lepton kinematics:

$$q^0 \leqslant E_{li} - (E_{lf})_{min} = E_{li} - \sqrt{(|\vec{p}_{li}| - |\vec{q}|)^2 + M_{lf}^2} \ , \tag{A6}$$

$$q^0 \geqslant E_{li} - (E_{lf})_{max} = 0 \ . \tag{A7}$$

However, there are further constraints on q^0 for a given $|\vec{q}|$ due to the hadron kinematics. For given set of q^0, $|\vec{q}|$, $\cos(\measuredangle \hat{q}\hat{p}_{ni}^*) = (2q^0 p_{ni}^{*0} + q^2)/(2|\vec{q}||\vec{p}_{ni}^*|)$ has to be physical. This requires

$$|\cos(\measuredangle \hat{q}\hat{p}_{ni}^*)| \leqslant 1$$

$$\Longleftarrow \quad |\vec{p}_{ni}^*| \geqslant \left| \frac{|\vec{q}|}{2} - \frac{q^0}{2}\sqrt{1 - \frac{4M^{*2}}{q^2}} \right| \equiv p^- \ . \tag{A8}$$

25

Eq. (A8) gives a lower bound of $|\vec{p}^{\,*}_{ni}|$ which is also required to be below the Fermi surface: $|\vec{p}^{\,*}_{ni}| \leqslant p_F$. Combining $p_F \geqslant p^-$ and the constraints in Eqs. (A6) and (A7), we find

$$q^0_{min} = \max(\sqrt{(|\vec{q}| - p_F)^2 + M^{*2}} - E_F, 0) \,, \tag{A9}$$

$$q^0_{max} = \min(\sqrt{(|\vec{q}| + p_F)^2 + M^{*2}} - E_F, E_{li} - \sqrt{(|\vec{p}_{li}| - |\vec{q}|)^2 + M^2_{lf}}) \,. \tag{A10}$$

Moreover, the constraint $|\vec{p}^{\,*}_{nf}| \geqslant p_F$ is not present in the former discussion, but is taken care of in the numerical calculation.

Appendix B: kinematics for pion production

The kinematic variables are defined in Fig. 7 in the lab frame. Except for the π momentum k_π, all the others are defined in the Appendix A. The variables defined in other frames will be mentioned explicitly. First we have

$$\sigma = \int dV \frac{1}{2p^0_{li}} \int \frac{d^3\vec{p}^{\,*}_{nf}}{(2\pi)^3 2p^{*0}_{nf}} \frac{d^3\vec{k}_\pi}{(2\pi)^3 2k^0_\pi} \frac{d^3\vec{p}_{lf}}{(2\pi)^3 2p^0_{lf}} \frac{d^3\vec{p}^{\,*}_{ni}}{(2\pi)^3 2p^{*0}_{ni}}$$
$$\times (2\pi)^4 \delta^4(q + p^*_{ni} - p^*_{nf} - k_\pi) \sum_{s_f, s_i} |M_{fi}|^2 \,.$$

The constraints on $\vec{p}^{\,*}_{ni}$ and $\vec{p}^{\,*}_{nf}$, i. e. $|\vec{p}^{\,*}_{ni}| \leqslant p_F$ and $|\vec{p}^{\,*}_{nf}| \geqslant p_F$, are always implicit in the formula.

One way to think about the phase space is that: given specific values for q and p^*_{ni}, the final pion and nucleon invariant mass $M_{\pi n}$ are fixed, and then the degrees of freedom in Isobaric frame (final pion and nucleon's center mass frame) is the angle of $\vec{k}_{I\pi}$, i.e. $\Omega_{\vec{k}_{I\pi}}$. So we have

$$\int \frac{d^3\vec{p}^{\,*}_{nf}}{(2\pi)^3 2p^{*0}_{nf}} \frac{d^3\vec{k}_\pi}{(2\pi)^3 2k^0_\pi} (2\pi)^4 \delta^4(q + p^*_{ni} - p^*_{nf} - k_\pi)$$
$$= \int dM_{n\pi} d\Omega_{\vec{k}_{I\pi}} \frac{1}{(2\pi)^2} \frac{|\vec{k}_{I\pi}|}{2} \delta((q + p^*_{ni})^2 - M^2_{\pi n}) \,.$$

In the above, we have made use of the following identities:

$$M_{\pi n} \equiv \sqrt{M^{*2} + |\vec{k}_{I\pi}|^2} + \sqrt{M_\pi^2 + |\vec{k}_{I\pi}|^2} \,,$$

$$E_{I\pi} = \frac{M^2_{\pi n} - M^{*2} + M^2_\pi}{2M_{\pi n}} \qquad E_{Inf} = M_{\pi n} - E_{I\pi} \,,$$

$$\frac{dE_{I\pi}}{dM_{\pi n}} = \frac{E_{Inf}}{M_{\pi n}} \,.$$

Then analogous to the analysis in the quasi-elastic scattering case, we have

$$\int \frac{d^3 \vec{p}_{ni}^{\,*}}{(2\pi)^3 2p_{ni}^{*0}} \delta((q + p_{ni}^*)^2 - M_{\pi n}^2)$$

$$= \int \frac{dp_{ni}^{*0} d\phi_{\vec{p}_{ni}^{\,*}}}{4|\vec{q}|(2\pi)^3} \Big|_{\cos(\angle \hat{q}\hat{p}_{ni}^*) = (2q^0 p_{ni}^{*0} + q^2 + M^{*2} - M_{\pi n}^2)/2|\vec{q}||\vec{p}_{ni}^{\,*}|} \cdot$$

So finally:

$$\sigma = \int dV \frac{1}{2p_{li}^0} \int \frac{d^3 \vec{p}_{lf}}{(2\pi)^3 2p_{lf}^0} \int dM_{n\pi} d\Omega_{\vec{k}_{I\pi}} dp_{ni}^{*0} d\phi_{\vec{p}_{ni}^{\,*}} \frac{1}{(2\pi)^5} \frac{|\vec{k}_{I\pi}|}{8|\vec{q}|} \sum_{s_f, s_i} |M_{fi}|^2$$

$$= \int dV dq^0 d|\vec{q}| dM_{\pi n} dp_{ni}^{*0} d\phi_{\vec{p}_{ni}^{\,*}} d\Omega_{\vec{k}_{I\pi}} \frac{1}{(2\pi)^7} \frac{|\vec{k}_{I\pi}|}{32(p_{li}^0)^2} \sum_{s_f, s_i} |M_{fi}|^2 \ .$$

Next, we need to determine the boundary of phase space in terms of these variables. First, it is clear that no constraint needs to be applied to $\Omega_{\vec{k}_{I\pi}}$ and $\phi_{\vec{p}_{ni}^{\,*}}$. Second, for a given set of $\vec{q}, q^0$, and $M_{\pi n}$, to make sure $|\cos(\angle \hat{q}\hat{p}_{ni}^*)| \leqslant 1$, there is a constraint on p_{ni}^{*0} besides $p_{ni}^{*0} \leqslant E_F$:

$$-2|\vec{q}||\vec{p}_{ni}^{\,*}| - q^2 \leqslant 2q^0 p_{ni}^{*0} + M^{*2} - M_{\pi n}^2 \leqslant 2|\vec{q}||\vec{p}_{ni}^{\,*}| - q^2 \ ,$$

$$\Longleftrightarrow \begin{cases} (|\vec{p}_{ni}^{\,*}| + \frac{\lambda+1}{2}|\vec{q}|)^2 + \frac{M^{*2}(q^0)^2}{q^2} - \frac{(\lambda+1)^2}{4}(q^0)^2 \geqslant 0 \ , & \lambda \equiv \frac{M_{\pi n}^2 - M^{*2}}{-q^2} \ ; \\ q^0 \sqrt{|\vec{p}_{ni}^{\,*}|^2 + M^{*2}} + |\vec{q}||\vec{p}_{ni}^{\,*}| \geqslant -\frac{q^2}{2} + \frac{M_{\pi n}^2 - M^{*2}}{2} \ , \end{cases}$$

$$\Longleftrightarrow |\vec{p}_{ni}^{\,*}| \geqslant p^- \equiv \left| \frac{\lambda+1}{2}|\vec{q}| - \frac{q^0}{2}\sqrt{(\lambda+1)^2 - \frac{4M^{*2}}{q^2}} \right| \ . \tag{B1}$$

Third, for a given set of $\vec{q}, q^0$, there is a constraint on $M_{\pi n}$, such that $p^- \leqslant p_F$. From $M_{\pi n}^2 \equiv q^2 + M^{*2} + 2q^0 p_{ni}^{*0} - 2|\vec{q}||\vec{p}_{ni}^{\,*}| \cos(\angle \hat{q}\hat{p}_{ni}^*)$, we have

$$q^2 + M^{*2} + 2q^0 E_F - 2|\vec{q}|p_F \leqslant M_{\pi n}^2 \leqslant q^2 + M^{*2} + 2q^0 E_F + 2|\vec{q}|p_F \ .$$

And to open the pion production threshold, we need

$$(M_\pi + M^*)^2 \leqslant M_{\pi n}^2 \ ,$$

So, we have

$$\max((M_\pi + M^*)^2, q^2 + M^{*2} + 2q^0 E_F - 2|\vec{q}|p_F)$$

$$\leqslant M_{\pi n}^2 \leqslant q^2 + M^{*2} + 2q^0 E_F + 2|\vec{q}|p_F \ . \tag{B2}$$

27

Fourth, for a given $|\vec{q}|$, there is a constraint on q^0 such that $(M_{\pi n})_{min} \leqslant (M_{\pi n})_{max}$. We have

$$q^2 + M^{*2} + 2q^0 E_F + 2|\vec{q}|p_F \geqslant (M_\pi + M^*)^2$$

$$\Longleftrightarrow \quad q^0 \geqslant \max(\sqrt{(M_\pi + M^*)^2 + (|\vec{q}| - p_F)^2} - E_F, 0) \,. \tag{B3}$$

However, there are further constraints on q^0 due to the lepton kinematics, which has been shown in Eqs. (A6) and (A7). Together with Eq. (B3), we have the boundary of q^0:

$$q^0_{max} = E_{li} - \sqrt{(|\vec{p}_{li}| - |\vec{q}|)^2 + M^2_{lf}} \,, \tag{B4}$$

$$q^0_{min} = \max(\sqrt{(M_\pi + M^*)^2 + (|\vec{q}| - p_F)^2} - E_F, 0) \,. \tag{B5}$$

Eqs. (A4) and (A5) give constraints on $|\vec{q}|$. And there are further constraints due to hadron kinematics. We have to make sure that $q^0_{max} \geqslant q^0_{min}$. But it is complicated to obtain an analytic expression for $|\vec{q}|$ based on this constraint. In the numerical calculations, we made use of another boundary assuming a static nucleon in the vacuum. Then, we can say the allowed region of $|\vec{q}|$ is always inside the previous region. Solving $q^0_{max} \geqslant q^0_{min}$ with $p_F = 0$ and $M^* = M$ gives us:

$$|\vec{q}| \leqslant \frac{\beta_A \frac{M_A^2 + (M_\pi + M)^2 - M_{lf}^2}{E_{li} + M} + \sqrt{\Delta}}{2(1 - \beta_A^2)} \,, \tag{B6}$$

$$|\vec{q}| \geqslant \frac{\beta_A \frac{M_A^2 + (M_\pi + M)^2 - M_{lf}^2}{E_{li} + M} - \sqrt{\Delta}}{2(1 - \beta_A^2)} \,. \tag{B7}$$

In the above,

$$\beta_A = \frac{E_{li}}{E_{li} + M} \,,$$

$$M_A = \sqrt{(E_{li} + M)^2 - E_{li}^2} \,,$$

$$\Delta = \frac{(M_A^2 + (M_\pi + M)^2 - M_{lf}^2)^2}{(E_{li} + M)^2} - 4(1 - \beta_A^2)(M_\pi + M)^2 \,.$$

So, Eqs. (A4), (A5), (B6) and (B7) are the bounds used in the numerical calculations. And to map out the physical region, we simply try and check. It is also complicated to determine an analytic expression for the threshold value of E_{li} in the LFG model. However, it is simpler to work out the value for pion production off a static nucleon, which is

$$E_{li} \geqslant \frac{(M_\pi + M + M_{lf})^2 - M^2}{2M} \,.$$

So, the difference between the true threshold and the value calculated above is essentially the binding energy.

---

[1] B. D. Serot and X. Zhang, Advances in Quantum Field Theory, Sergey Ketov, ed. (InTech, Croatia, 2012), ch. 4.

[2] B. D. Serot and X. Zhang, Phys. Rev. C *in press* [arXiv:1206.3812].

[3] B. D. Serot and J. D. Walecka, Adv. Nucl. Phys. **16**, (1986) 1.

[4] B. D. Serot and J. D. Walecka, Int. J. Mod. Phys. E **6**, (1997) 515.

[5] R. J. Furnstahl, B. D. Serot, and H.-B. Tang, Nucl. Phys. A **615**, (1997) 441; **640**, (1998) 505 (E).

[6] R. J. Furnstahl and B. D. Serot, Nucl. Phys. A **671**, (2000) 447.

[7] R. J. Furnstahl and B. D. Serot, Nucl. Phys. A **673**, (2000) 298.

[8] R. J. Furnstahl and B. D. Serot, Comments Mod. Phys. **2**, (2000) A23.

[9] B. D. Serot, Lecture Notes in Physics **641**, G. A. Lalazissis, P. Ring, and D. Vretenar, eds. (Springer, Berlin Heidelberg, 2004), p. 31.

[10] B. D. Serot, Ann. of Phys. **322**, (2007) 2811.

[11] M. A. Huertas, Phys. Rev. C **66**, 024318 (2002); **67**, (2003) 019901 (E).

[12] M. A. Huertas, Acta Phys. Polon. B **34**, (2003) 4269.

[13] M. A. Huertas, Acta Phys. Polon. B **35**, (2004) 837.

[14] J. McIntire, Acta Phys. Polon. B **35**, (2004) 2261.

[15] J. McIntire, arXiv:nucl-th/0507006.

[16] J. D. Walecka, Theoretical Nuclear and Subnuclear Physics, second ed. (World Scientific, Singapore, 2004), ch. 24.

[17] J. McIntire, Y. Hu, and B. D. Serot, Nucl. Phys. A **794**, (2007) 166.

[18] Y. Hu, J. McIntire, and B. D. Serot, Nucl. Phys. A **794**, (2007) 187.

[19] J. McIntire, Ann. of Phys. **323**, (2008) 1460.

[20] B. D. Serot, Phys. Rev. C **81**, (2010) 034305.

[21] A. A. Aguilar-Arevalo *et al.*, (MiniBooNE Collaboration), Phys. Rev. Lett. **98**, (2007) 231801.

[22] A. A. Aguilar-Arevalo *et al.*, (MiniBooNE Collaboration), Phys. Rev. Lett. **102**, (2009) 101802.

[23] A. A. Aguilar-Arevalo *et al.*, (MiniBooNE Collaboration), Phys. Rev. Lett. **105**, (2010) 181801.

[24] T. Katori (for the MicroBooNE collaboration), AIP Conf. Proc. **1405**, (2011) 250.

[25] J. A. Harvey, C. T. Hill, and R. J. Hill, Phys. Rev. Lett. **99**, (2007) 261601.

[26] J. A. Harvey, C. T. Hill, and R. J. Hill, Phys. Rev. D **77**, (2008) 085017.

[27] Richard J. Hill, Phys. Rev. D **81**, (2010) 013008.

[28] S. S. Gershtein, Yu. Ya. Komachenko, and M. Yu. Khlopov, Sov. J. Nucl. Phys. **33**, (1981) 860.

[29] M. Martini, M. Ericson, G. Chanfray and J. Marteau, Phys. Rev. D **80**, (2009) 065501.

[30] S. Nakayama *et al.*, (K2K Collaboration), Phys. Lett. B **619**, (2005) 255.

[31] M. Hasegawa *et al.*, (K2K Collaboration), Phys. Rev. Lett. **95**, (2005) 252301.

[32] R. Gran *et al.*, (K2K Collaboration), Phys. Rev. D **74**, (2006) 052002.

[33] A. Rodriguez *et al.*, (K2K Collaboration), Phys. Rev. D **78**, (2008) 032003.

[34] K. Hiraide *et al.*, (SciBooNE Collaboration), Phys. Rev. D **78**, (2008) 112004.

[35] A. A. Aguilar-Arevalo *et al.*, (MiniBooNE Collaboration), Phys. Rev. Lett. **100**, (2008) 032301.

[36] A. A. Aguilar-Arevalo *et al.*, (MiniBooNE Collaboration), Phys. Lett. B **664**, (2008) 41.

[37] A. A. Aguilar-Arevalo *et al.*, (MiniBooNE Collaboration), Phys. Rev. Lett. **103**, (2009) 081801.

[38] A. V. Butkevich, Phys. Rev. C **78**, (2008) 015501.

[39] A. V. Butkevich, Phys. Rev. C **80**, (2009) 014610.

[40] S. K. Singh and E. Oset, Nucl. Phys. A **542**, (1992) 587.

[41] S. K. Singh and E. Oset, Phys. Rev. C **48**, (1993) 1246.

[42] A. Meucci, C. Giusti, and F. D. Pacati, Nucl. Phys. A **739**, (2004) 277.

[43] A. Meucci, C. Giusti, and F. D. Pacati, Nucl. Phys. A **744**, (2004) 307.

[44] J. Nieves, J. E. Amaro, and M. Valverde, Phys. Rev. C **70**, (2004) 055503; **72**, (2005) 019902 (E).

[45] M. C. Martinez *et al.*, Phys. Rev. C **73**, (2006) 024607.

[46] T. Leitner, L. Alvarez-Ruso, and U. Mosel, Phys. Rev. C **73**, (2006) 065502.

[47] T. Leitner, L. Alvarez-Ruso, and U. Mosel, Phys. Rev. C **74**, (2006) 065502.

[48] T. Leitner, O. Buss, L. Alvarez-Ruso, and U. Mosel, Phys. Rev. C **79**, (2009) 034601.

[49] A. Kartavtsev, E. A. Paschos, and G. J. Gounaris, Phys. Rev. D **74**, (2006) 054007.

[50] C. Praet, O. Lalakulich, N. Jachowicz, and J. Ryckebusch, Phys. Rev. C **79**, (2009) 044603.

[51] T. Leitner, U. Mosel and S. Winkelmann, Phys. Rev. C **79**, (2009) 057601.

[52] S. K. Singh, M. J. Vicente-Vacas, and E. Oset, Phys. Lett. B **416**, (1998) 23; **423**, (1998) 428 (E).

[53] T. Sato, D. Uno, and T. S. H. Lee, Phys. Rev. C **67**, (2003) 065201.

[54] B. Szczerbinska, T. Sato, K. Kubodera, and T. S. Lee, Phys. Lett. B **649**, (2007) 132.

[55] J. E. Amaro, M. B. Barbaro, J. A. Caballero, T. W. Donnelly, A. Molinari, and I. Sick, Phys. Rev. C **71**, (2005) 015501.

[56] J. A. Caballero, J. E. Amaro, M. B. Barbaro, T. W. Donnelly, C. Maieron, and J. M. Udias, Phys. Rev. Lett. **95**, (2005) 252502.

[57] J. E. Amaro, M. B. Barbaro, J. A. Caballero, and T. W. Donnelly, Phys. Rev. Lett. **98**, (2007) 242501.

[58] M. Martini, G. Co', M. Anguiano, and A. M. Lallena, Phys. Rev. C **75**, (2007) 034604.

[59] J. E. Amaro, M. B. Barbaro, J. A. Caballero, T. W. Donnelly, and J. M. Udias, Phys. Rev. C **75**, (2007) 034613.

[60] M. V. Ivanov, M. B. Barbaro, J. A. Caballero, A. N. Antonov, E. Moya de Guerra, and M. K. Gaidarov, Phys. Rev. C **77**, (2008) 034612.

[61] A. Gil, J. Nieves and E. Oset, Nucl. Phys. A **627**, (1997) 543.

[62] W. M. Alberico, M. Ericson, and A. Molinari, Ann. of Phys. **154**, (1984) 356.

[63] E. Oset, L.L. Salcedo, Nucl. Phys. A **468**, (1987) 631.

[64] R. Rosenfelder, Ann. of Phys. **128**, (1980) 188.

[65] K. Wehrgerger, C. Bedau, and F. Beck, Nucl. Phys. A **504**, (1989) 797.

[66] K. Wehrgerger, and R. Wittman, Nucl. Phys. A **513**, (1990) 603.

[67] T. Herbert, K. Wehrgerger, and F. Beck, Nucl. Phys. A **541**, (1992) 699.

[68] K. Wehrgerger, Phys. Rept. **225**, (1993) 273.

[69] M. J. Dekker, P. J. Brussaard, and J. A. Tjon, Phys. Rev. C **49**, (1994) 2650.

[70] A. De Pace, M. Nardi, W. M. Alberico, T. W. Donnelly, and A. Molinari, Nucl. Phys. A **726**, (2003) 303.

[71] S. X. Nakamura, T. Sato, T.-S. H. Lee, B. Szczerbinska, and K. Kubodera, Phys. Rev. C **81**, (2010) 035502.

[72] Y. Horikawa, M. Thies, and F. Lenz, Nucl. Phys. A **345**, (1980) 386.

[73] S. L. Adler, S. Nussinov and E. A. Paschos, Phys. Rev. D **9**, (1974) 2125.

[74] E.A. Paschos, L. Pasquali and J.Y.Yu, Nucl. Phys. B **588**, (2000) 263.

[75] D. Casper, Nucl. Phys. Proc. Suppl. **112**, (2002) 161.

[76] A. A. Aguilar-Arevalo *et al.*, (MiniBooNE Collaboration), Phys. Rev. D **81**, (2010) 092005.

[77] P. Barreau *et al.*, Nucl. Phys. A **402**, (1983) 515.

[78] J. S. O'Connell *et al.*, Phys. Rev. C **35**, (1987) 1063.

[79] M. Hirata, J. H. Koch, F. Lenz and E. J. Moniz, Ann. of Phys. **99**, (1976) 374.

[80] J. Boguta, Phys. Lett. B, **109**, (1982) 251.

[81] D. S. Kosov, C. Fuchs, B. V. Martemyanov, Amand Faessler, Phys. Lett. B **421**, (1998) 37.

[82] R. J. Furnstahl, John J. Rusnaka and B. D. Serot, Nucl. Phys. A **632**, (1998) 607.

[83] I. J. D. MacGregor *et al.*, Phys. Rev. Lett. **80**, (1998) 245.

[84] J. Nieves, E. Oset, and C. Garcia-Recio, Nucl. Phys. A **554**, (1993) 554.

[85] *Private communication with T. W. Donnelly.*